Inorganic Chemistry
Article

Inorg. Chem. **2009**, *48*, 5141–5153 **5141**
DOI: 10.1021/ic900082u

Synthesis, Short-Range Structure, and Electrochemical Properties of New Phases in the Li−Mn−N−O System

Jordi Cabana,[†,‡] Nicolas Dupré,[‡,§] Frédéric Gillot,[†,∥] Alan V. Chadwick,[⊥] Clare P. Grey,[‡] and M. Rosa Palacín*[,†]

[†]*Institut de Ciència de Materials de Barcelona (CSIC) Campus UAB, E-08193 Bellaterra, Catalonia, Spain,* [‡]*Chemistry Department, State University of New York at Stony Brook, New York 11794-3400,* [§]*Institut des Matériaux Jean Rouxel, 44322 Nantes Cedex 3, France,* [∥]*Laboratoire de Réactivité et de Chimie des Solides, Université de Picardie Jules Verne, 80039 Amiens, France, and* [⊥]*Functional Materials Group, School of Physical Sciences, University of Kent, Canterbury, Kent CT2 7NH, U.K.*

Received January 15, 2009

A crystal-chemical exploration of part of the Li−Mn−N−O system was carried out. Several samples were synthesized using Li_3N, Mn_xN and Li_2O and characterized with chemical analysis, XRD, XAS, and NMR. An increase in the starting proportion of Li_2O increases the amounts of lithium and oxygen in the compounds, but, according to the XANES Mn *K*-edge spectra, all the oxynitrides still contain Mn^{5+} ions preferentially coordinated by N^{3-}, forming [MnN_4] tetrahedra. The analysis of the position of these samples in the compositional $Li_3N-Li_2O-MnN_x$ ternary phase diagram and the plot of their cell parameters against the oxygen molar fraction indicates that all the oxynitrides belong to the same tie-line, which also includes Li_2O but not Li_7MnN_4. Although the XRD patterns suggest that these samples crystallize in a disordered antifluorite-type structure, the analysis of the ^{6}Li NMR data indicates that short-range ordering does exist. The performance as electrode materials in lithium batteries of the synthesized samples was also evaluated. $Li_{7.9}MnN_{3.2}O_{1.6}$ was shown to be the most attractive candidate because of its higher capacity values and improved retention upon cycling with respect to the other members of the series.

Introduction

Nitrogen is the most abundant component of the Earth's atmosphere, but we live in a world of oxides because their stability is, in general, much higher than that of nitrides. The explanation lies in the unfavorable electronic affinity of nitrogen (1736 kJ/mol for $N \rightarrow N^{3-}$ vs 601 kJ/mol for $O \rightarrow O^{2-}$)[1] and the high-energy bond of the diatomic molecule (945 kJ/mol for N_2 vs 493 kJ/mol for O_2),[2] which makes it less reactive. As a consequence, studying nitrided compounds requires the use of complex synthetic and handling methods to overcome these issues. Indeed, it is mainly because of the progress achieved in this field that our knowledge about nitride chemistry has substantially increased in the last 15 years.[3−9] Interesting properties have been reported for these compounds,[10] and structural similarities have been found with known oxides, opening the possibility for solid solutions to be designed and prepared in which the O/N ratio is used to tune the properties of the resulting materials. It is quite likely that the resulting oxynitrides have, among other features, improved air stability with respect to the parent nitrides.

Although the number of studies devoted to oxynitride crystal-chemistry[3] is still smaller than that for nitrides, different examples are available in the literature of phases with possible applications in photocatalysis,[11−13] photoluminescence,[14] dielectrics,[15] and as non-toxic inorganic pigments,[16]

*To whom correspondence should be addressed. E-mail: rosa.palacin@icmab.es.

(1) Pearson, R. G. *Inorg. Chem.* **1991**, *30*, 2856–2858.
(2) Buschow, K. H. J.; Cahn, R. W.; Flemings, M. C.; Ilschner, B.; Kramer, E. J.; Mahajan, S. *Encyclopedia of Materials: Science and Technology*; Pergamon: Amsterdam, 2001; Vol. *7*, p 6161.
(3) Marchand, R.; Laurent, Y.; Guyader, J.; L'Haridon, P.; Verdier, P. *J. Eur. Ceram. Soc.* **1991**, *8*, 197–213.
(4) Brese, N. E.; O'Keeffe, M. Crystal Chemistry of Inorganic Nitrides. In *Structure and bonding*; Clark, M. J., Ed.; Springer Verlag: Berlin, 1992; Vol. *79*, pp 307−378.
(5) DiSalvo, F. J.; Clarke, S. J. *Curr. Opin. Solid State Mater. Sci.* **1995**, *1*, 241–249.
(6) Niewa, R.; Jacobs, H. *Chem. Rev.* **1996**, *96*, 2053–2062.
(7) Gregory, D. H. *J. Chem. Soc., Dalton Trans.* **1999**, 259–270.
(8) Niewa, R.; DiSalvo, F. J. *Chem. Mater.* **1998**, *10*, 2733–2752.
(9) Zerr, A.; Riedel, R.; Sekine, T.; Lowther, J. E.; Ching, W. Y.; Tanaka, I. *Adv. Mater.* **2006**, *18*, 2933–2948.
(10) Oyama, S. T. *J. Solid State Chem.* **1992**, *96*, 442–445.
(11) Asahi, R.; Morikawa, T.; Ohwaki, T.; Aoki, K.; Taga, Y. *Science* **2001**, *293*, 269–271.
(12) Hitoki, G.; Takata, T.; Kondo, J. N.; Hara, M.; Kobayashi, H.; Domen, K. *Chem. Commun.* **2002**, 1698–1699.
(13) Maeda, K.; Teramura, K.; Lu, D. L.; Takata, T.; Saito, N.; Inoue, Y.; Domen, K. *Nature* **2006**, *440*, 295–295.
(14) Soignard, E.; Machon, D.; McMillan, P. F.; Dong, J. J.; Xu, B.; Leinenweber, K. *Chem. Mater.* **2005**, *17*, 5465–5472.
(15) Kim, Y. I.; Woodward, P. M.; Baba-Kishi, K. Z.; Tai, C. W. *Chem. Mater.* **2004**, *16*, 1267–1276.
(16) Jansen, M.; Letschert, H. P. *Nature* **2000**, *6781*, 980–982.

Published on Web 04/30/2009

or negative electrode[17] and electrolyte[18] materials in Li-ion batteries. Interestingly, some lithium-containing oxynitrides such as $Li_{16}M_2N_8O$ (M = Nb, Ta),[19−21] $Li_{14}Cr_2N_8O$,[22,23] $Li_6Ca_{12}Re_4N_{16}O_3$[24] or $Li_2Sr_6Cr_2N_8O$[25] were discovered because of small accidental oxygen leaks in the reaction setup intended in principle for the preparation of nitrides. Two main methods have been described for the synthesis of these phases. The first one (and the most usual) consists of the ammonolysis of oxide mixtures at high temperatures.[16,26−32] The other approach was proposed by Juza and co-workers in the 1950s, when they investigated the possibility of controlling the amount of oxygen in lithium transition metal oxynitrides by adding variable quantities of binary oxides to a mixture of Li_3N and a transition metal, which was subsequently heated under a nitrogen atmosphere. They used this methodology to prepare what they described as solid solutions of a lithium transition metal nitride having a general formula $Li_{2n-1}MN_n$ (where M = transition metal) and Li_2O. More specifically, systems with M = Ti,[33] V,[34] and Cr[35] were studied. In all cases, the corresponding ternary nitrides adopt different antifluorite type superstructures derived from Li/M ordering in the tetrahedral positions of the structure, whereas the oxynitrides show a disordered antifluorite structure, with a $Fm\bar{3}m$ space group. Recent studies by other authors[22] and ourselves[36] in the Li−Cr−N−O system point out that this solid solution might not have the ternary nitride as end member, as suggested by the existence of $Li_{14}Cr_2N_8O$, a compound with an antifluorite superstructure due to Li/Cr and N/O ordering, and its co-existence with the fully disordered $Li_{10}CrN_4O_2$ phase depending on the initial reagent ratio and the synthesis conditions.[36] A limited solid solution range also appears to be the case for the Li−Ti−N−O system,[37] yet more controversy has arisen as to whether Li_7VN_4 is a member of the $Li_7VN_4 \cdot nLi_2O$ solid solution or not.[37−40]

To our knowledge, no such systematic study has been carried out in the Li−Mn−N−O system, where the only phase known, $Li_{7.9}MnN_{3.2}O_{1.6}$, was recently reported by us.[41] This compound also has an antifluorite structure and constitutes a very good example of the effect of the anionic ratio on the properties of oxynitrides. When compared to Li_7MnN_4, higher air stability was found,[17] albeit a certain sensitivity to moisture was still observed. Nonetheless, $Li_{7.9}MnN_{3.2}O_{1.6}$ could be stored for several weeks without noticeable decomposition when kept in a dry atmosphere.

Lithium transition metal nitrides were first proposed in the 1990s as alternative materials for negative electrodes in lithium-ion batteries. Among them, $Li_{3-x}Co_xN$ shows excellent specific capacity values,[42,43] that is, the amount of charge obtained per unit mass of material used, whereas Li_7MnN_4 shows smaller capacity values but notable retention upon cycling.[44−47] $Li_{7.9}MnN_{3.2}O_{1.6}$ was the first lithium transition metal oxynitride tested for this application. Its initial specific capacity is comparable to that of the nitride, but it shows improved retention on cycling.[17]

As a logical extension of our previous work, we present here the results of the exploration of the Li−Mn−N−O system by changing both the Li/Mn and the N/O ratios simultaneously through the introduction of variable amounts of Li_2O to the reaction mixture. Our aim has been to obtain deeper insight into the chemical and structural relationships among the phases found in this system by using techniques such as powder X-ray diffraction (XRD), X-ray absorption spectroscopy (XAS), and solid state Nuclear Magnetic Resonance (NMR). In addition, representative samples were tested as electrodes in lithium batteries, and the effects of the compositional changes on the performance of these compounds are also discussed.

Experimental Section

Samples with different Li, Mn, N, and O contents were prepared from a powder mixture of Li_3N (Aldrich), manganese nitride (Mn_xN, commercial mixture of Mn_4N and Mn_2N, with $x = 3.1$, according to chemical analysis, Cerac Inc. 99.9%) and Li_2O (Aldrich, 97%) in different proportions, as shown in Table 1. The samples were pelletized and treated at 800 °C for 8 h under nitrogen flow (Carburos Metálicos 99.9995% additionally purified passing through a Supelco gas purifier). Li_7MnN_4 was synthesized from

(17) Cabana, J.; Dupré, N.; Grey, C. P.; Subias, G.; Caldés, M. T.; Marie, A. M.; Palacín, M. R. *J. Electrochem. Soc.* **2005**, *152*, A2246–A2255.
(18) Bates, J. B.; Dudney, N. J.; Gruzalski, G. R.; Zuhr, R. A.; Choudhury, A.; Luck, C. F.; Robertson, J. D. *J. Power Sources* **1993**, *43*, 103–110.
(19) Chen, X. Z.; Eick, H. A. *J. Solid State Chem.* **1996**, *127*, 19–24.
(20) Bois, L.; L'Haridon, P.; Wiame, H.; Grange, P. *Mater. Res. Bull.* **1998**, *33*, 9–19.
(21) Wachsmann, C.; Brokamp, T.; Jacobs, H. *J. Alloys Compd.* **1992**, *185*, 109–119.
(22) Gudat, A.; Haag, S.; Kniep, R.; Rabenau, A. *Z. Naturforsch. B.* **1990**, *45*, 111–120.
(23) Akhmetzyanov, T. M.; Obrosov, V. P.; Batalov, N. N.; Plaksin, S. V.; Martem'yanova, Z. S.; Tamm, V. K. *Russian J. Electrochem.* **1993**, *29*, 1187–1188.
(24) Hochrein, O.; Kniep, R. *Z. Anorg. Allg. Chem.* **2001**, *627*, 301–303.
(25) Hochrein, O.; Kniep, R. *Z. Anorg. Allg. Chem.* **2002**, *628*, 1–3.
(26) Pors, F.; Marchand, R.; Laurent, Y. *J. Solid State Chem.* **1993**, *107*, 39–42.
(27) Assabaa-Boultif, R.; Marchand, R.; Laurent, Y. *Eur. J. Solid State Inorg. Chem.* **1995**, *32*, 1101–1113.
(28) Tobías, G.; Oró-Solé, J.; Beltrán-Porter, D.; Fuertes, A. *Inorg. Chem.* **2001**, *40*, 6867–6869.
(29) Clarke, S. J.; Guinot, B. P.; Michie, C. W.; Calmont, M. J. C.; Rosseinsky, M. J. *Chem. Mater.* **2002**, *14*, 288–294.
(30) Clarke, S. J.; Chalker, P. R.; Holman, J.; Michie, C. W.; Puyet, M.; Rosseinsky, M. J. *J. Am. Chem. Soc.* **2002**, *124*, 3337–3342.
(31) Tessier, F.; Marchand, R. *J. Solid State Chem.* **2003**, *171*, 143–151.
(32) Tobías, G.; Beltrán-Porter, D.; Lebedev, O. I.; Van Tendeloo, G.; Rodriguez-Carvajal, J.; Fuertes, A. *Inorg. Chem.* **2004**, *43*, 8010–8017.
(33) Juza, R.; Uphoff, W.; Gieren, W. *Z. Anorg. Allg. Chem.* **1957**, *292*, 71–81.
(34) Juza, R.; Gieren, W.; Haug, J. *Z. Anorg. Allg. Chem.* **1959**, *300*, 61–71.
(35) Juza, R.; Haug, J. *Z. Anorg. Allg. Chem.* **1961**, *309*, 276–282.
(36) Cabana, J.; Ling, C. D.; Oró-Solé, J.; Gautier, D.; Tobías, G.; Adams, S.; Canadell, E.; Palacín, M. R. *Inorg. Chem.* **2004**, *43*, 7050–7060.
(37) Cabana, J.; Mercier, C.; Gautier, D.; Palacín, M. R. *Z. Anorg. Allg. Chem.* **2005**, *631*, 2136–2141.
(38) Niewa, R.; Zherebtsov, D.; Hu, Z. *Inorg. Chem.* **2003**, *42*, 2538–2544.
(39) Niewa, R.; Zherebtsov, D. A. *Z. Anorg. Allg. Chem.* **2006**, *632*, 387–388.
(40) Palacín, M. R. *Z. Anorg. Allg. Chem.* **2006**, *632*, 389.
(41) Cabana, J.; Rousse, G.; Fuertes, A.; Palacín, M. R. *J. Mater. Chem.* **2003**, *13*, 2402–2404.
(42) Nishijima, M.; Kagohashi, T.; Imanishi, M.; Takeda, Y.; Yamamoto, O.; Kondo, S. *Solid State Ionics* **1996**, *83*, 107–111.
(43) Shodai, T.; Okada, S.; Tobishima, S.; Yamaki, J. *J. Power Sources* **1997**, *68*, 515–518.
(44) Nishijima, M.; Takodoro, N.; Takeda, Y.; Imanishi, N.; Yamamoto, O. *J. Electrochem. Soc.* **1994**, *141*, 2966–2971.
(45) Suzuki, S.; Shodai, T. *Solid State Ionics* **1999**, *116*, 1–9.
(46) Cabana, J.; Rousse, G.; Palacín, M. R. In *New Trends in Intercalation Compounds for Energy Storage and Conversion*; Julien, C., Zaghib, K., Prakash, J., Eds.; PV2003-20, The Electrochemical Society Proceeding Series: Paris, 2003; pp 139−146.
(47) Cabana, J.; Dupré, N.; Rousse, G.; Grey, C. P.; Palacín, M. R. *Solid State Ionics* **2005**, *176*, 2205–2218.

Table 1. Amount of Reagents Used for the Synthesis and Stoichiometry, Obtained after Chemical Analysis, of the Different Samples Prepared in This Study

sample number	mole Li_2O	mole $Mn_{3.1}N$	mole Li_3N	stoichiometry
1	3.1	1	7.6	$Li_{7.9}MnN_{3.2}O_{1.6}$
2	4.7	1	7.6	$Li_9MnN_{3.3}O_{2.1}$
3	6.3	1	7.6	$Li_{10.9}MnN_{3.6}O_{2.6}$
4	7.9	1	8.2	$Li_{11.9}MnN_{3.7}O_3$
5	9.5	1	7.6	$Li_{12.6}MnN_{3.5}O_{3.6}$
6	11.0	1	7.6	$Li_{13.9}MnN_{3.4}O_{4.3}$
7	12.6	1	8.4	$Li_{14.9}MnN_{3.5}O_{4.7}$
8	14.2	1	8.9	$Li_{16.5}MnN_{3.7}O_{5.2}$
9	15.8	1	8.7	$Li_{17.1}MnN_{3.6}O_{5.7}$
10	25.2	1	12.1	$Li_{24}MnN_{3.5}O_{9.2}$
11	31.5	1	12.6	$Li_{28.7}MnN_{3.6}O_{11.5}$
12	37.8	1	15.8	$Li_{34.2}MnN_{3.9}O_{13.7}$
13	47.4	1	19.0	$Li_{42.5}MnN_{4.3}O_{17.3}$
14	53.3	1	21.9	$Li_{47.8}MnN_{4.1}O_{20.3}$
15	63.0	1	25.2	$Li_{55.6}MnN_{4.4}O_{23.7}$

homogeneous mixtures of lithium nitride and manganese nitride in mole ratio 7.6:1 at 650 °C for 6 h, also under nitrogen flow. Finally, Li_3MnO_4 was synthesized as reported elsewhere,[48] by heating 2:1 mixtures of $LiOH \cdot H_2O$ and $LiMnO_4 \cdot H_2O$ under air in increments of 10 °C from 70 to 125 °C, where the temperature was held for 1 h, followed by a final heating at 170 °C for 2−3 h. All manipulations involving air sensitive compounds were performed in an Ar-filled glovebox.

The manganese and lithium contents were determined by Inductively Coupled Plasma-Optical Emission Spectroscopy (ICP-OES) after acid hydrolysis of the sample. Nitrogen content was obtained from elemental analysis through combustion in oxygen atmosphere using an EA 1108 Carlo Erba Instruments analyzer. Oxygen content could not be analyzed, as the available analysis techniques such as the inert gas fusion method yield high deviations from the actual values when both oxygen and nitrogen contents are high.[36]

Powder X-ray Diffraction patterns were obtained with a PANalytical X'Pert PRO theta/theta diffractometer (Cu $K\alpha_1, \lambda = 1.5406$). To avoid decomposition of the air sensitive samples, they were loaded in 0.3 mm capillaries inside the glovebox and sealed under argon. The CELREF (v. 3) program[49] has been used to refine the cell parameters of the obtained samples.

XAS measurements were performed on station 7.1 at the CLRC Daresbury Synchrotron Radiation Source, with an electron energy of 2 GeV, at an average current of 150 mA. Station 7.1 is equipped with a double Si (111) crystal monochromator that can be offset from the Bragg angle to reject harmonic contaminants from the monochromatic beam. In the present work the harmonic rejection was set at 50%. Mn *K* edge XAS spectra were collected at room temperature in conventional transmission mode using gas-filled reference and signal ion chamber detectors. A third ion chamber was used to collect the XAS of a metal foil placed after the signal ion chamber to provide a reference for the calibration of the edge position for each scan. Spectra were typically collected to $k = 16$ Å^{-1}, and several scans were taken to improve the signal-to-noise ratio. The samples were prepared by thoroughly mixing the powder with a binder polymer (dibutyl phthalate, DBP) and a few drops of acetone. After drying the viscous mixture, the resulting paste was cast onto the inside of an aluminum-laminated plastic bag. The bag was then hot-sealed to protect the samples from contact with moisture. The amount of sample was adjusted to give an adsorption of about $\mu d = 1$. Finally, the data were processed using the Daresbury suite of XAS programs EXCALIB, EXBACK (or EXBROOK), and EXCURV98.[50,51]

^{6}Li Magic Angle Spinning Nuclear Magnetic Resonance (MAS NMR) experiments were performed at an operating frequency of 29.45 MHz on a CMX-200 spectrometer, that is, a field strength (B_0) of 4.7 T, using a 1.8 mm inside diameter probe manufactured by Dr. A. Samoson and co-workers (KBFI, Tallinn, Estonia). The spectra were acquired with a rotor synchronized echo sequence ($\pi/2$-τ-π-τ-acq.), where $\tau = 1/\nu_r$ and ν_r is the spinning frequency. A $\pi/2$ pulse width of 2.7 μs and a pulse delay of 0.2 s were used with a spinning frequency (ν_r) of 35 kHz.

Electrochemical lithium intercalation/deintercalation tests were performed in two-electrode Swagelok cells using lithium foil (Aldrich 99.9%) as a counter electrode. The working electrode consisted of a powder mixture of the selected sample with 15% Super P carbon black (kindly supplied by MMM, Belgium). Two sheets of Whatman GF/D borosilicate glass fiber soaked with 1 M $LiPF_6$ were used as a separator, and the cells were tested using a MacPile potentiostat (Biologic, France) in galvanostatic mode at C/10 rate (defined here as 0.1 lithium/hour).

Results and Discussion

Synthesis. Variable amounts of Li_3N, Li_2O, and Mn_xN ($x \approx 3.1$) were used to synthesize the different samples presented in this work, as indicated in Table 1. When no Li_2O was added to the reaction mixture, Li_7MnN_4, with an ordered antifluorite structure ($P\bar{4}3n$ space group), could be prepared at 650 °C during 6 h under purified nitrogen gas, as previously reported.[46,47] However, when the Li_3N/Mn_xN ratio in the nitride was maintained, but Li_2O was added to the mixture to induce the formation of oxynitrides, both the temperature and the treatment time had to be raised (up to 800 °C and 8 h, respectively) to avoid the formation of mixtures of Li_7MnN_4 and an oxynitride. This is shown in Figure 1 (see pattern labeled "T = 650°C") for a sample with the same initial reagent proportions as sample 1 (corresponding to the previously reported composition, $Li_{7.9}MnN_{3.2}O_{1.6}$)[17,41] but heated at 650 °C instead. The XRD patterns of representative impurity-free oxynitride samples are also shown in Figure 1, together with that of Li_7MnN_4 for comparison. As expected, they are consistent with a disordered antifluorite structure.

A lower limit to the amount of Li_2O that could be reacted with the starting Li_3N-Mn_xN mixture was found. When 1.5 mols were added per mole of Mn_xN, a diffractogram similar to that obtained at lower temperature was obtained (see "Low Li_2O" in Figure 1). Although the peaks, at first glance, can be indexed with a Li_7MnN_4-like supercell, those at 32°, 38°, 55°, 65°, and 85°, 2θ, which also correspond to the (111), (200), (220), (311), (222), and (400) reflections, respectively, in a disordered structure with $Fm\bar{3}m$ space group, have much higher relative intensities than those seen in pure Li_7MnN_4. In addition, close examination of the peak at 55° reveals the

(48) Saint, J. A.; Doeff, M. M.; Reed, J. *J. Power Sources* **2007**, *172*, 189–197.

(49) See http://www.ccp14.ac.uk/tutorial/lmgp/celref.htm.

(50) Binsted, N.; Campbell, J. W.; Gurman, S. J.; Stephenson, P. C. *SERC Daresbury Program Library*; Daresbury Laboratory: Warrington, U.K., 1992.

(51) Binsted, N. *EXCURV98*; CCLRC Daresbury Laboratory: Warrington, U.K., 1998.

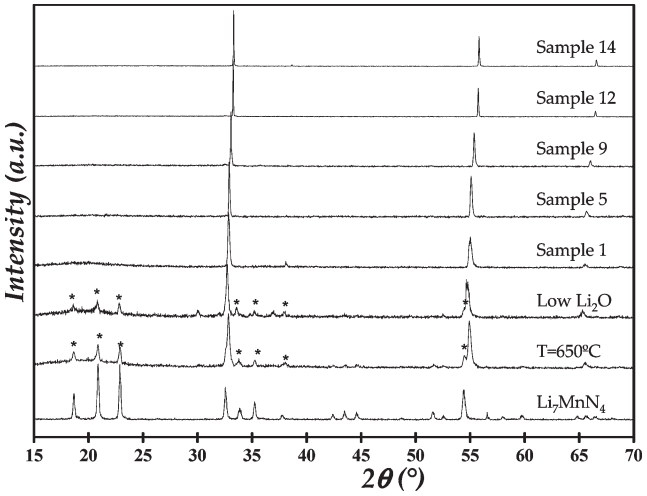

Figure 1. X-ray Diffraction (XRD) patterns of selected samples prepared in this study (see labels), acquired with Cu $K\alpha_1$ radiation (λ = 1.5406). The asterisks mark the peaks corresponding to the existence of an antifluorite superlattice as a secondary phase.

existence of a small shoulder (marked with an asterisk), which could be indexed as the (440) reflection in the Li_7MnN_4 supercell. This suggests that there may not be a continuous transition from an ordered to a disordered structure but co-existence of two phases when the oxygen content is small. Similar tendencies have already been observed in our previous studies of samples with low oxygen content both in the Li−V−N−O and Li−Ti−N−O systems.[37]

When 12 or more moles Li_2O were added in the starting mixture, extra Li_3N was required to avoid remaining impurities of $(Li,Mn)_2N$ and Li_2O in the final product. The supplementary amount needed increases sharply when the initial values of Li_2O are high, that is, beyond 25 moles of Li_2O per mole of $Mn_{3.1}N$. When the contents of the alkaline oxide were very high, pure samples could not be synthesized even by increasing the Li_3N content considerably, and only mixtures of Li_2O and a lithium manganese oxynitride were obtained.

A progressive change in the color of the samples from dark gray to dark green was observed as the initial Li and O contents increased, consistent with the tendency observed for related Li−M−N−O systems.[37,52] Such behavior has also been described in other oxynitride phases,[31,53,54] and has gained great interest because of the possible application of these type of compounds in the field of inorganic pigments[16,55] because of the absence of toxic metals.

To evaluate the air stability of these compounds and probe any possible changes with the oxygen content, they were stored outside the Ar-filled glovebox and XRD measurements were made after 2 and 8 weeks. The results for samples 1, 4, and 12 are shown in Figure 2 as an example. Sample 1, which corresponds to the previously published $Li_{7.9}MnN_{3.2}O_{1.6}$ phase was shown to be more air stable than Li_7MnN_4, specially under dry atmosphere conditions.[17] The stability of sample 4 is comparable, but sample 12 shows a surprisingly high air sensitivity, leading to the formation of $LiOH \cdot H_2O$ even after only 1 week outside the glovebox. Therefore, samples with oxygen contents higher than that in $Li_{7.9}MnN_{3.2}O_{1.6}$ do not show improved stability, most likely because their chemical properties are very similar to those of pure Li_2O, which undergoes quick hydration and carbonation and needs to be stored under a controlled atmosphere.

X-ray Absorption Spectroscopy (XAS). Information on the oxidation state and local environment of the manganese ions in this series can be obtained from Mn *K* edge XANES. Figure 3a shows the normalized spectra of samples 2, 7, 8, 9, 10, and 14 while Figure 3b shows the first derivative. All spectra are similar and exhibit a strong pre-peak structure at 6534 eV, in good agreement with our previous studies on $Li_{7.9}MnN_{3.2}O_{1.6}$ and Li_7MnN_4.[17] This prepeak is ascribed to 1s → 3d transitions, its intensity being strongly dependent on the site symmetry. Its occurrence is a clear indication that the manganese atoms are tetrahedrally coordinated in all cases, as expected from the antifluorite-type structure of these compounds.

The energy position of the main edge (defined as the first inflection point in the derivative spectra) is often used as an indication of the oxidation state of the observed transition metal, higher states leading to higher energy shifts with respect to the metal foil reference.[56] However, this position is also affected by the degree of covalency of the bond between the metal and the surrounding anions.[57] In fact, a noticeable shift of the main edge between oxides and nitrides containing transition metals in the same formal oxidation states, the latter appearing at lower energies, has been reported by other authors.[38,58] Such discrepancies were also observed when comparing Li_7MnN_4 and $Li_{7.9}MnN_{3.2}O_{1.6}$, which were shown to contain Mn^{5+} according to earlier magnetic susceptibility measurements,[41,59] to a series of manganese oxides; the main edge position of the nitrided compounds was very similar, but it was also shown to be closer to that of MnO_2 than to Na_3MnO_4.[17] This is explained on the basis of the Mn^{5+} cations being surrounded by N^{3-} anions in Li_7MnN_4 and $Li_{7.9}MnN_{3.2}O_{1.6}$, as opposed to the more ionic Mn−O bonds existing in the Mn^{5+} oxide.

The Li−Mn−N−O samples prepared in this study contain increasing amounts of oxygen. Thus, if the distribution of ions in their structure were random, as could be deduced from the XRD patterns, an increase in oxide ions in the $[MnX_4]$ tetrahedra would be expected. If the manganese oxidation state did not change along the series, the result would be a shift in the main edge position of the XANES spectra. However, this is not the case, as these spectra overlap (Figure 3). Therefore, if an increasing amount of O^{2-} is present around the manganese ions, the absence of shift would necessarily be

(52) Cabana, J., Antifluorite-type transition metal nitrides and oxynitrides: Synthesis, characterization and application in Lithium batteries. Ph.D. Thesis dissertation, Universitat Autònoma de Barcelona, Bellaterra, Spain, 2004.
(53) Diot, N.; Larcher, O.; Marchand, R.; Kempf, J. Y.; Macaudière, P. *J. Alloys Compd.* **2001**, *323*−*324*, 45–48.
(54) Chevire, F.; Tessier, F.; Marchand, R. *Eur. J. Inorg. Chem.* **2006**, 1223–1230.
(55) Tessier, F.; Maillard, P.; Chevire, F.; Domen, K.; Kikkawa, S. *J. Ceram. Soc. Jpn.* **2009**, *117*, 1–5.
(56) Belli, M.; Scafati, A.; Bianconi, A.; Mobilio, S.; Palladino, L.; Reale, A.; Burattini, E. *Solid State Commun.* **1980**, *35*, 355–361.
(57) Hu, Z.; Kaindl, G.; Meyer, G. *J. Alloys Compd.* **1997**, *246*, 186–192.
(58) Niewa, R.; Hu, Z.; Kniep, R. *Eur. J. Inorg. Chem.* **2003**, *2003*, 1632–1634.
(59) Niewa, R.; Wagner, F. R.; Schnelle, W.; Hochrein, O.; Kniep, R. *Inorg. Chem.* **2001**, *40*, 5215–5222.

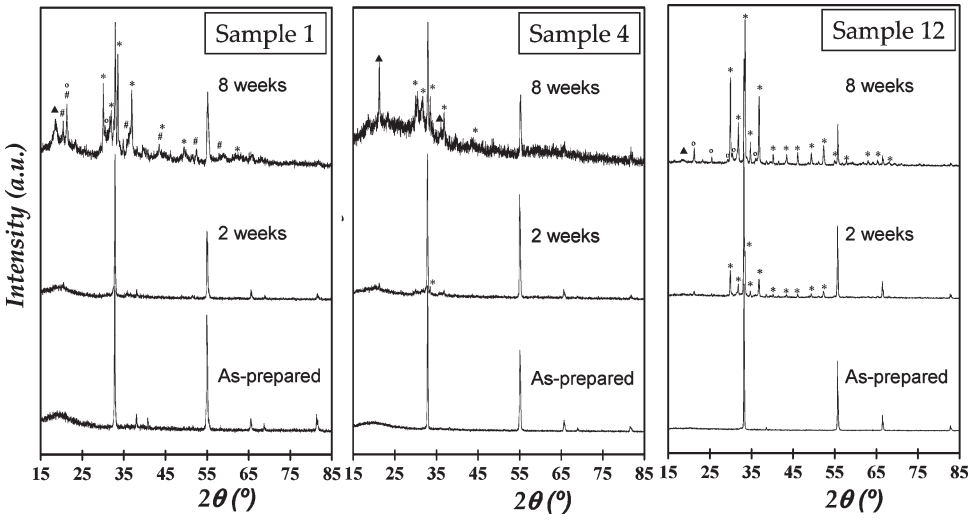

Figure 2. XRD patterns of samples 1, 4, and 12, collected with Cu Kα_1 radiation (λ = 1.5406) after different periods of time, as labeled in the figure, while stored in open air instead of under argon atmosphere in a glovebox. The phases resulting from their chemical decomposition are indicated with the following symbols:(*) $LiOH \cdot H_2O$; (○) Li_2CO_3; (▲) MnO; (#) $LiMn_2O_4$.

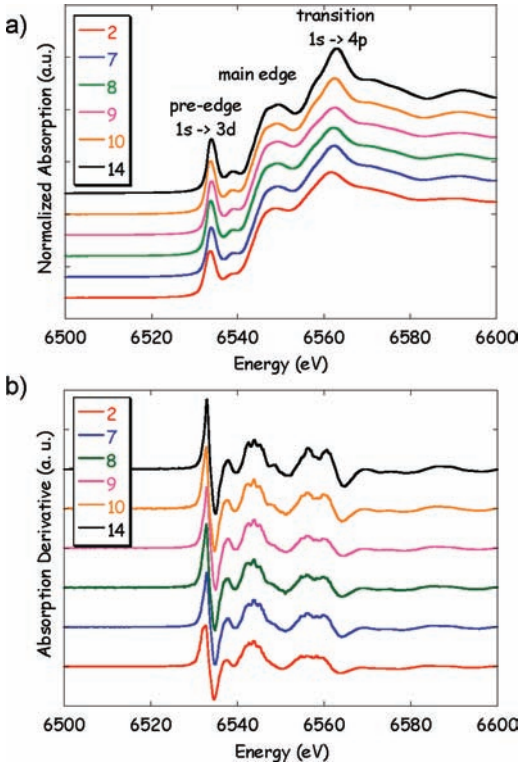

Figure 3. (a) Normalized Mn *K*-edge XANES spectra at room temperature of selected samples prepared in this study (see labels); (b) first derivative of the normalized XANES spectra.

an indication of a decrease in the oxidation state of manganese. Alternatively, this absence of shift could be ascribed to a strong tendency of Mn^{5+} ions to be coordinated by nitrogen instead of oxygen, thus leading to the existence of covalent $[MnN_4]$ structural units, such as those in Li_7MnN_4, in all the compounds. This latter situation has already been experimentally observed in related Li−M−N−O (M = transition metal) systems that crystallize in a ordered antifluorite structure, such as $Li_{14}Cr_2N_8O$,[22,36] $Li_{16}Nb_2N_8O$,[19] or $Li_{16}Ta_2N_8O$[21] for which powder neutron and single crystal X-ray diffraction studies revealed the existence of ordered $[MN_4]$ and $[LiN_{1-x}O_x]$ units. Further, a general tendency for the highest charged anion (N^{3-} in this case) to preferentially coordinate the cations with the highest oxidation state (Mn^{5+} in this case) has already been reported for several oxyanion systems.[60] As a result of this previous knowledge, the second situation (Mn^{5+} almost exclusively coordinated by N^{3-}) is considered to be the most plausible. This would imply that the structure of these samples is not completely disordered, consistent with the incommensurate structure previously proposed for $Li_{7.9}MnN_{3.2}O_{1.6}$ based on powder neutron diffraction and high resolution transmission electron microscopy (HRTEM) results.[17]

Stoichiometry of the Samples and Phase Diagram. The stoichiometries obtained from chemical analysis can also be found in Table 1. As mentioned in the Experimental Section, the oxygen content could not be determined because techniques such as the inert gas fusion method proved to produce systematic errors when the amount of nitrogen is high. To estimate this magnitude in the samples, we fixed the nitrogen, lithium, and manganese contents based on the analytical results, and assumed that they all contain Mn^{5+}, in agreement with the XANES results. These results indicate a tendency to somewhat higher oxygen contents in the prepared products than in the initial reaction mixtures. Besides the inherent experimental error, this is ascribed to a small amount of impurities either coming from the nitrogen gas, even when using a purifier, or because of small leaks in the supply (note that, to have a continuous flow of nitrogen, the reaction setup cannot be made with sealed tubes), which react with the very air sensitive reagents employed.

As expected, the Li/Mn ratio and the oxygen content increase with the introduction of Li_2O. The molar nitrogen content is similar in the first 11 samples indicating that the extra Li_3N required to achieve purity for higher initial Li_2O contents was only needed to compensate for different evaporation rates of this reagent at 800 °C. However, this tendency seems to change in the last 5 samples, where the results show an increasing amount of

(60) Fuertes, A. *Inorg. Chem.* **2006**, *45*, 9640–9642.

nitrogen in the structure. This suggests that, even if its evaporation is still the main reason why extra Li_3N needs to be added, additional lithium in the form of the binary nitride could also be needed for the formation of the oxynitride.

The stoichiometries obtained by chemical analysis indicate, despite the experimental error, that samples 1 to 11 are cationic deficient with respect to the ideal cation/anion ratio 2:1 of the antifluorite structure. These vacancies can be electrochemically filled reversibly by lithium, as we have formerly reported for sample 1 ($Li_{7.9}MnN_{3.2}O_{1.6}$).[17] Indeed, contrary to the parent systems with other transition metals such as Ti[37,61] or V,[34,37,38] the presence of vacancies suggests again that these oxynitrides cannot be written as a solid solution between the parent nitride (Li_7MnN_4 in this case) and Li_2O, both compounds having a vacancy-free antifluorite structure. The cation/anion ratio for samples 12 to 15 seems to be much closer to 2, which would be consistent with an absence of cationic vacancies. This implies that as Mn and N are diluted in the structure, the resulting samples have strong crystal-chemical similarities with Li_2O, consistent with their behavior upon storage in air reported above.

The stoichiometries obtained for all the samples can be used to draw a ternary phase diagram involving Li_3N, Li_2O, and a hypothetical Mn^{5+} nitride (MnN_x with $x \sim 1.7$) to account for the nitrogen uptake from the flowing gas. The resulting diagram is shown in Figure 4a. The position of Li_7MnN_4 in the Li_3N-MnN_x axis is also indicated, together with the tie-line for the hypothetical vacancy-free solid solution $Li_7MnN_4 \cdot xLi_2O$ (or $yLi_7MnN_4 \cdot (1 - y)Li_2O$, where $y = 1/(1 + x)$). Interestingly, this theoretical line does not fit the points corresponding to the samples prepared. In contrast, if a tie-line defined by the experimental compositions is drawn, then the crossing point in the Li_3N-MnN_x axis does not correspond to Li_7MnN_4 but to a hypothetical composition "$Li_{4.5}MnN_{3.2}$", implying that this would be the actual end member of the system. Attempts to synthesize this compound were unsuccessful, and only mixtures of Li_7MnN_4 and $(Li,Mn)_2N$[62] were obtained. Furthermore, previous compositional exploration of the Li−Mn−N system[59] did not provide any evidence of the existence of such a compound. Contrary to these observations on one end of the tie-line, the other end does seem to reach the corner defined by Li_2O, confirming that it belongs to the same compositional range.

The cell parameters of all the phase-pure samples (1 to 15) are plotted in Figure 4b against the oxygen molar fraction. Data for Li_2O (JCPDS file No. 12-0254) and Li_7MnN_4 (defined as $a' = 0.5(a_{Li_7MnN_4})$ to allow the direct comparison with the simple antifluorite unit cell of the oxynitride samples) are also included as references. The points corresponding to the oxynitrides can be fitted by a linear function, thus adding further evidence that they belong to the same tie-line in the ternary phase diagram. The cell parameter of Li_2O also falls inside the line defined by our samples, whereas that of Li_7MnN_4 would clearly

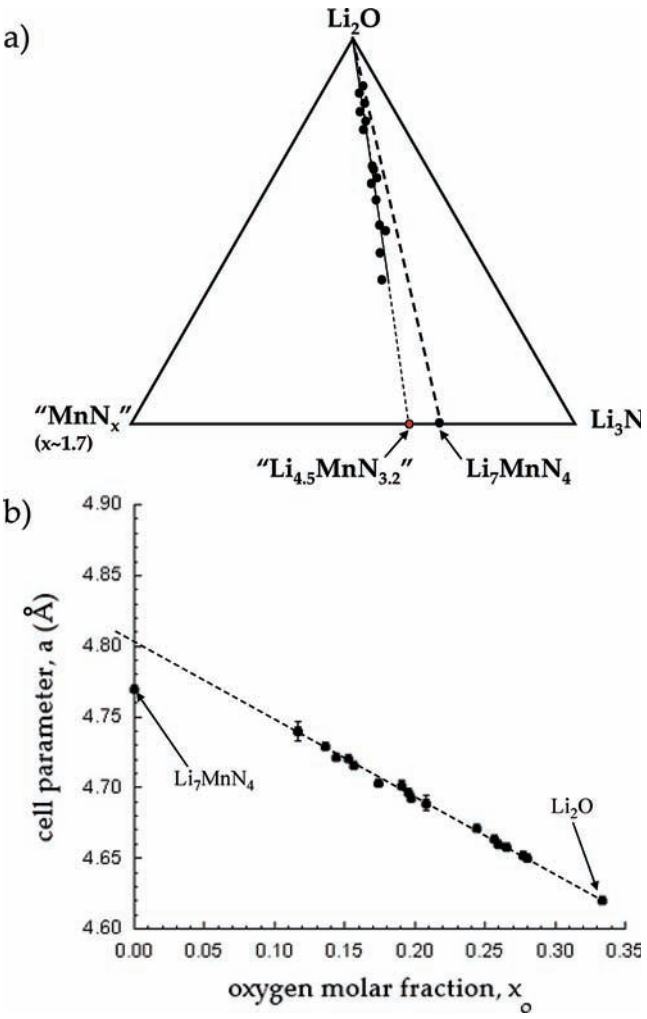

Figure 4. (a) Ternary phase diagram, Li_2O−Li_3N−$MnN_{1.7}$, showing the compositional points resulting from the stoichiometries obtained from the chemical analysis of the samples prepared as part of this study. The points corresponding to Li_7MnN_4 and a hypothetical nitride with formula $Li_{4.5}MnN_{3.2}$ (see text) are indicated. (b) Cell parameter evolution of the samples prepared in this study plotted vs their oxygen molar fraction. The two extremes, $x = 0.0$ and $x = 1/3$, correspond to Li_7MnN_4 and Li_2O, respectively.

be out, as it is too low, confirming that none of the samples belong to the hypothetical $yLi_7MnN_4 \cdot (1 - y)Li_2O$ solid solution. In contrast, if the linear function that fits all the other points is traced and extended to the y axis, the cell parameter of the hypothetical end member, "$Li_{4.5}MnN_{3.2}$", can be extrapolated to be around $a = 4.80$ Å, considering an ideal and disordered antifluorite unit cell.

^{6}Li MAS NMR Studies on the Evolution of the Short-Range Ordering. Our XRD data seem to indicate that the lithium manganese oxynitrides have a simple antifluorite structure due to both Li−Mn and N−O disorder in the cationic and anionic positions, respectively. However, our earlier studies on $Li_{7.9}MnN_{3.2}O_{1.6}$ demonstrated that the situation is more complex, since an incommensurate structure due to partial ordering was observed in the Neutron Diffraction (ND) and HRTEM results.[17] Our ^{6}Li MAS NMR data of this compound also pointed to the existence of a degree of short-range ordering, since a small number of discrete of resonances were observed corresponding to clearly favored local environments. As an extension of previous NMR work, and to better evaluate

(61) Juza, R.; Weber, H. H.; Meyer-Simon, E. *Z. Anorg. Allg. Chem.* **1953**, *273*, 48–64.
(62) Niewa, R.; DiSalvo, F. J.; Yang, D.-K.; Zax, D. B.; Luo, H.; Yelon, W. B. *J. Alloys Compd.* **1998**, *266*, 32–38.

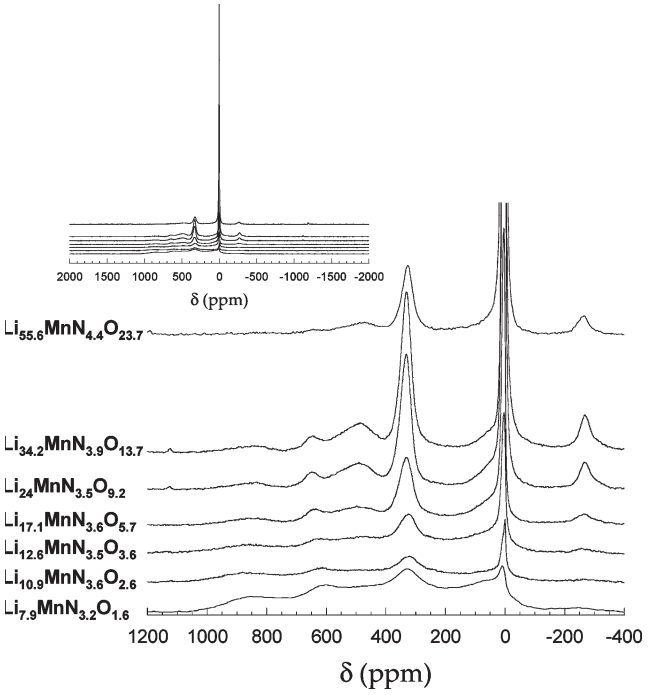

Figure 5. Zoom showing the isotropic resonances in the NMR spectra of selected samples in the Li−Mn−O−N system prepared in this study, acquired at a spinning speed of 35 kHz, normalized to the amount of sample in the rotor. The 3 ppm resonances are truncated in the Li rich samples. The full spectra are shown as an inset to the figure.

the possible cationic ordering in these phases, spectra were collected for all the samples. Those considered representative are shown in Figure 5.

Some general trends can be observed when analyzing the series. All the spectra contain broad peaks in the range from −500 to 1300 ppm, with a sharper one at 3 ppm. In the samples with low lithium/oxygen contents, the considerable width of the peaks is an indication of the existence of a variety of environments and, thus, a notable degree of structural disorder.

Lithium NMR shifts in compounds with paramagnetic centers (Mn^{5+} in this case) are typically large and nonzero. They are generally generated by the existence of Li−X−M (where X = anion, M = transition metal) contacts, which lead to hyperfine (if the interaction is with the unpaired electrons of the metal, as in this study) or Knight (if the compound is metallic and, thus, the interaction is with the conduction electrons) shifts.[63] Shifts of around 0 ppm are ascribed to interactions involving only diamagnetic ions in direct contact with lithium via an anion. These can either arise from impurities existing in the samples or be due to lithium environments in the compound that only contain diamagnetic ions in their coordination sphere. In our case, since no observable impurities were found by XRD, the noticeable intensity of the peak near 0 ppm, together with the fact that it grows as the samples are more dilute in manganese, indicates that it is mainly associated to lithium ions with no manganese nearby within the oxynitride structure. Nonetheless, a contribution from a small amount of impurities cannot be ruled out since NMR is often much more sensitive to their presence than XRD.

A reduction of the relative area underneath the different peaks generated by lithium surrounded by one (or several) Mn ion(s) is evident as the Mn content decreases, further confirming their assignment to local environments involving the transition metal. However, the behavior of different individual peaks is not identical. For instance, those at −260 and 330 ppm get sharper with higher Li/Mn ratios, while there is a very strong decrease of the resonances at 850 and 600 ppm that reveals two new resonances at 476 and 637 ppm. These resonances are likely also present for the samples with lower lithium (and oxygen) contents, albeit not resolvable above the background. Finally, the shoulder at 60 ppm that can be readily observed for $Li_{7.9}MnN_{3.2}O_{1.6}$ (sample 1) also shows a decrease in intensity and almost disappears beneath the 3 ppm resonance at very high lithium/oxygen contents.

All the phases prepared in this paper have an antifluorite-type structure with the cations in tetrahedral coordination, and the anions in cubic environments. As a result, the cations will have 3 different types of interactions with the other nearby 22 cations, via the 4 intervening anions (Figure 6, right inset), distributed as follows: 6 cations leading to 2 Li−X−M (M = metal, X = anion) contacts with bond angles of 70° each (green spheres); 12 cations leading to 1 Li−X−M interaction with a bond angle of 109° each (blue spheres); and 4 cations forming one 180° bond each (yellow spheres). The angle of the Li−X−M interactions is of the utmost importance because it determines the size and sign of the resulting hyperfine shift.[63,64] On the basis of a previous analysis of the ^{6}Li NMR spectra of Li_7MnN_4,[47] 70° Li−N−Mn interactions are predicted to lead to a large positive shift, whereas a smaller but still positive shift is predicted for the 109° Li−N−Mn interactions, and, finally, a negative interaction is predicted for 180° Li−N−Mn bonds. Unfortunately, the distortions of the ideal bond geometry generated by the cationic ordering in Li_7MnN_4 leads to a variety of Li−N−Mn angles and distances that hindered the univocal assignment of a shift value to each of these 3 basic types of interactions.

The spectrum of the most dilute sample, $Li_{55.6}MnN_{4.4}O_{23.7}$ (sample 15), was used as a starting point for the assignment of lithium environments to the resonances in the spectra because of its simplicity. Assuming that manganese is always surrounded by nitrogen based on the XAS results, a model with a purely statistical distribution of cations and anions can be ruled out. If we consider a statistical distribution of manganese and lithium in the 22 positions available in the cation coordination sphere of Li, about 68% of the lithium environments will contain no manganese, whereas about 27% and 5% will contain one and two manganese ions, respectively, with the combined probability for more than two being small, well below 1%. Since the intensity ratio of the NMR signals is proportional to the relative amount of each environment in the compound, this statistical distribution results in a spectrum dominated by a resonance at approximately 0 ppm, with three resonances of intermediate intensity (one for each non-equivalent position that one

(63) Grey, C. P.; Dupré, N. *Chem. Rev.* **2004**, *104*, 4493–4512.

(64) Carlier, D.; Ménétrier, M.; Grey, C. P.; Delmas, C.; Ceder, G. *Phys. Rev. B* **2003**, *67*, 14.

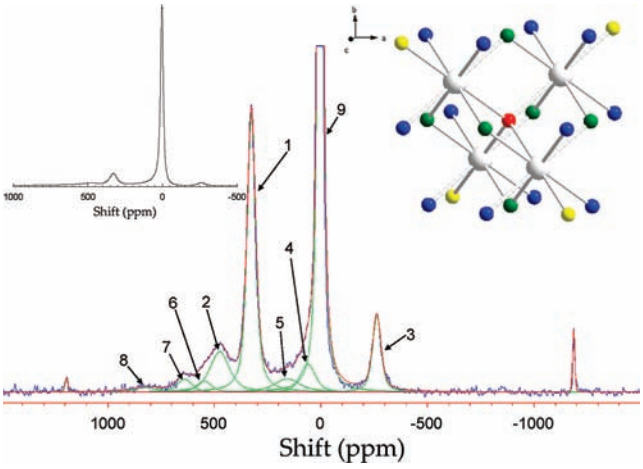

Figure 6. Zoom-in and spectral deconvolution (green, peaks and red, sum) of the NMR spectrum (blue line) of $Li_{55.6}MnN_{4.4}O_{23.7}$ (sample 15), acquired at a spinning speed of 35 kHz. Left inset: view of the full spectrum. Right inset: Scheme of the first anionic (large white spheres) and cationic coordination shell of a cation (red sphere) in the ideal antifluorite structure. The three different possible types of cationic positions that lead to M−X−M (M = metal, X = anion) forming angles of 70°, 109°, and 180° are indicated by green, blue, and yellow spheres, respectively.

Table 2. Results of the Decomposition of the NMR Spectrum of $Li_{55.6}MnN_{4.4}O_{23.7}$, and Assignment of the Resonances Assuming a Structural Model with Manganese Ions Preferentially Coordinated by Nitrogen (See Text)[a]

			assignment		
peak number	shift (ppm)	relative intensity	Mn at 70°	Mn at 109°	Mn at 180°
1	328 ± 1	13.0	0	1	0
2	476 ± 2	4.3	1	0	0
3	−261 ± 1	3.5	0	0	1
4	62 ± 20	2.8	0	1	1
5[b]	150 ± 10	1.8	0	2	2
6	637 ± 7	1.0	0	2	0
7	552 ± 7	0.9	1	1	1
8	820 ± 15	0.6	1	1	0
9	3 ± 1	72.6	0	0	0

[a] The peak number corresponds to the labels in Figure 6. The intensity of the sidebands was added to their corresponding isotropic peak. The values were normalized so that the total intensity of the spectrum is 100. Estimations of the error in the shifts are given based on the comparison of several independent deconvolution iterations. Variations of about ±1 were found for the relative intensity values. [b] This resonance can also be assigned to Li−O−Mn environments (see text).

manganese can adopt in the cationic shell), and a series of much weaker ones associated to the presence of two manganese ions, all of them with large absolute shift values.

Because of the lack of information on the number of non-equivalent lithium sites (environments) present in the phase, the deconvolution of the spectrum (Figure 6 and Table 2) was performed using the minimum number of peaks to lead to the best fit. Several independent deconvolution iterations were performed and always led to a total of eight peaks with non-zero shifts. Given the proportion of sites with different Li−X−Mn angles in the antifluorite structure (6:12:4 for one Mn at 70°:109°:180°), we assign the three most prominent resonances, at 476, 328, and −261 ppm, with a relative intensity ratio of 4.3:13.0:3.5, to the Li^+ environments with one Mn at 70°, 109°, and 180°, respectively, consistent with our previous rationalization of the sign and size of the shifts for these interactions.[47] Using these values, an assignment of the other resonances present in the spectrum of $Li_{55.6}MnN_{4.4}O_{23.7}$ can be made. The broad peak at 637 ppm (peak 7) and the very weak one at 820 ppm (peak 8) can respectively be assigned to a lithium environment with two manganese ions at 109°, and another one with one manganese ion at 109° and a second one at 70°. Additionally, shoulders are detected to higher frequencies of the 476 ppm resonance (peak 2), at 552 ppm (peak 6), and of the diamagnetic peak, at 62 ppm (peak 4). The former is predicted to be the result of lithium environments with three manganese ions in the cationic coordination shell, each in one of the three possible positions, leading to 70°, 109°, and 180° interactions. The latter is assigned to lithium ions with one 109° and one 180° Li−N−Mn interaction. Finally, the inclusion of a weak resonance at 150 ppm (peak 5) in the deconvolution was necessary to account for the high baseline between the two largest peaks of the spectrum. While, in principle, this peak could be assigned to an environment with four manganese ions, two at 109° and two at 180°, this would imply a large number of manganese ions around one lithium ion. The diluted content of the transition metal in this sample makes this somewhat counterintuitive. In addition, the large width of this resonance raises the question as to whether there might indeed be composed of more than one peak.

In general, the majority of the NMR resonances of $Li_{55.6}MnN_{4.4}O_{23.7}$ can be satisfactorily assigned when assuming that the lithium and manganese ions are always in contact through nitrogen, validating this initial assumption and supporting our conclusions resulting from the Mn XAS data. Nonetheless, other possibilities for the assignment of the different NMR peaks were explored by analyzing the spectrum of Li_3MnO_4, an oxide containing Mn^{5+}. This compound adopts an ordered variant of wurtzite, where both cations and anions are in tetrahedral coordination, and has two crystallographic positions for lithium (Figure 7, inset).[65] This is consistent with the observation of 2 discrete resonances, at 686 and 616 ppm, in the ^{6}Li NMR spectrum (Figure 7), which is reported here for the first time. The broad shoulder at 477 ppm is ascribed to an impurity of $LiMn_2O_4$. On the basis of the relative intensity ratio of the two peaks (1.8:1 for the 686:616 ppm resonances) and the ratio of multiplicities in the crystallographic structure (2:1 Li1:Li2), the assignment of the 686 and 616 ppm sites to Li1 and Li2, respectively, is clear-cut. Both peaks arise from lithium environments with four $Li^+-O^2-Mn^{5+}$ contacts of around 109°−118° accounting for their similar shifts, the 70 ppm difference resulting from small differences in bond distance and angle. Given the additive character of the shifts, we conclude that each ∼109° interaction in this compound accounts for 150−175 ppm. The lower magnitude than that obtained for a $Li^+-N^{3-}-Mn^{5+}$ interaction (328 ppm) is consistent with the more covalent character of the latter and the consequent enhanced transfer of spin density though a stronger orbital overlap. The existence of a peak at 160 ppm in the spectrum of

(65) Meyer, G.; Hoppe, R. *Z. Anorg. Allg. Chem.* **1976**, *424*, 249–256.

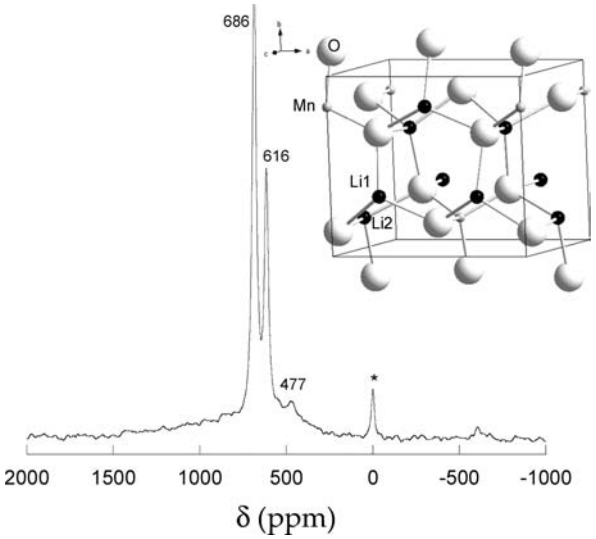

Figure 7. NMR spectrum of Li_3MnO_4, acquired at 38 kHz. The isotropic shift values for the two Li sites in the structure are indicated. The broad peak at 477 ppm is the result of a $LiMn_2O_4$ impurity, whereas the asterisk indicates the existence of a diamagnetic impurity. Inset: Representation of the structure of Li_3MnO_4, as obtained from the literature.[65] The different atoms in the unit cell are labeled and the cell edges are indicated.

$Li_{55.6}MnN_{4.4}O_{23.7}$ suggests that, at very high oxygen contents, a small fraction of the manganese (not enough to produce a shift in the Mn *K* edge signal) could be partially surrounded by oxygen in environments such as $[MnN_3O]$. This may seem more plausible than the alternative assignment of this resonance to Li^+ surrounded by four Mn^{5+}.

The hyperfine shift values assigned to the $Li^+-N^{3-}-Mn^{5+}$ interactions at 70°, 109°, and 180° in an antifluorite-type oxynitride above can be used to calculate the shift that would be expected for each of the five lithium environments in the antifluorite-type superstructure of Li_7MnN_4,[47] based on the number of each type of interaction. These results can be compared to the assignments previously made based on the site multiplicity-resonance intensity relationship. Li1 has two manganese ions at 75.3° (predicted shift: 476 ppm x2 = 952 ppm; assigned shift:[47] 1208 ppm); Li2 has four manganese ions at 119.6° (predicted shift: 328 ppm x4 = 1312 ppm; assigned shift: 347 ppm); Li3 has three manganese ions at 113° and one at 180° (predicted shift: 328 ppm x4 + (−261 ppm) x1 = 723 ppm; assigned shift: 597 ppm); Li4 has one manganese ion at 75.3°, at 111.7°, and at 173.6° (predicted shift: 476 ppm x1 + 328 ppm x1 + (−261 ppm) x1 = 543 ppm; assigned shift: 861 ppm); finally, Li5 has one manganese ion at 78.9°, and two at 110.7° (predicted shift: 476 ppm x1 + 328 ppm x2 = 1132 ppm; assigned shift: 1333 ppm). The discrepancies between assignments, most pronounced for the case of Li2, are, as expected, in part because of the strong and varied distortions from the ideal geometries induced by the cation ordering, which, as we have just described for Li_3MnO_4, have a dramatic effect on the hyperfine shifts. This also raises the question as to whether the Li2 resonance in Li_7MnN_4 is actually covered by a larger one at a different shift, and that the 347 ppm resonance, which, coincidentally, is the strongest in $Li_{7.9}MnN_{3.2}O_{1.6}$, is actually due to an impurity of a lithium manganese oxynitride. Both compounds have XRD reflections at very similar angles (see discussion of the XRD data above), and NMR is often more sensitive to weak impurities, indicating that this suggestion is plausible.

Table 3. Different Possible Combinations That Are Generated Because of the Presence of 2 Mn Ions in the 22 Cationic Positions Surrounding a Central Li Ion in the Antifluorite Structure and Their Corresponding Resonance Assignments, if Observed, in the ^{6}Li MAS NMR Spectrum $Li_{55.6}MnN_{4.4}O_{23.7}$ (See Table 2)[a]

number of Mn ions in each cationic position					
Mn at 70°	Mn at 109°	Mn at 180°	# possible combinations	assigned shift (ppm)	relative intensity
2	0	0	15		
0	2	0	66	637	23
0	0	2	6		
1	1	0	72	820	14
1	0	1	24		
0	1	1	48	62	63

[a] The experimentally observed relative intensity of each resonance with respect to the total intensity of peaks (normalized to 100) assigned to the presence of 2 Mn is given.

Additional information on the ordering in these lithium manganese oxynitride phases can be obtained by comparing the relative integrated intensities of the resonances because of the presence of two (or more) manganese ions in the cation coordination shell to their calculated probabilities (see Table 3). The two most probable environments in the random model correspond to lithium ions with two manganese ions at 109°, and with one manganese ion at 109° and another at 70°. However, according to our spectral deconvolution, the corresponding resonances, at 637 and 820 ppm, have lower relative intensity than, for instance, that at 62 ppm, which results from one manganese ion at 109° and another at 180°. The peak at 820 ppm is actually the smallest of those found in the whole deconvolution (Table 2), whereas, according to our calculations, it should be the largest of the resonances corresponding to environments with more than one manganese ion. The resonance at 552 ppm, which is ascribed to the existence of three manganese ions, also seems to be too large when compared to the sum of those due to two manganese (0.9% vs 3.8%, see Table 2), as opposed to the values of 0.6% and 5%, respectively, predicted above. All these observations provide evidence against a random ordering of manganese within the framework of the compound. Further, a qualitative comparison between the lithium environments resulting from different possible arrangements of two manganese ions in the three positions of the coordination shell (i.e., at 70°, 109°, or 180°) and the situation observed experimentally reveals that configurations with 1 Mn at 109° + 1 Mn at 180° are present in greater concentrations than predicted in the random model only when these two manganese ions are not in the each other's first cation coordination shell (i.e., forming 70° Mn−N−Mn bonds). The same conclusion can be reached based on the lower than predicted (based on the random model) intensity of the resonance associated to lithium environments with 2 Mn at 70°. Hence, our NMR results suggest that, as manganese is diluted in these compounds, it is partially ordered, at least at short-range, so as to increase the Mn−Mn distances

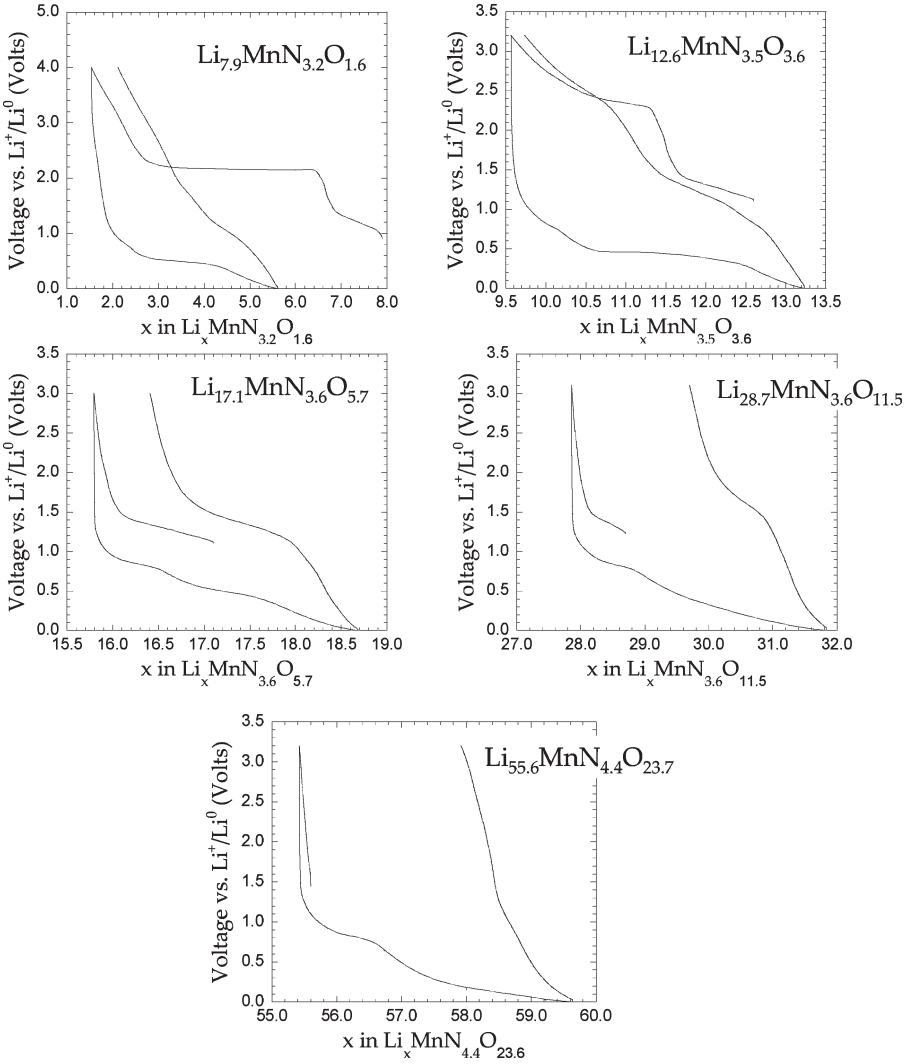

Figure 8. Voltage vs composition profiles of the first charge−discharge−charge sweeps of batteries containing selected samples prepared in this study as electrodes, tested against lithium metal in galvanostatic mode at C/10 rate. $Li_{7.9}MnN_{3.2}O_{1.6}$ (sample 1) was cycled between 4 and 0 V, sample 10 was cycled between 3 and 0 V, whereas $Li_{12.6}MnN_{3.5}O_{3.6}$, $Li_{17.1}MnN_{3.6}O_{5.7}$, $Li_{28.7}MnN_{3.6}O_{11.5}$, and $Li_{55.6}MnN_{4.4}O_{23.7}$ (samples 5, 9, 11, and 15, respectively) were cycled between 3.2 and 0 V.

and thus reduce Coulombic repulsions between these ions. N^{3-} most likely serves to screen the Mn^{5+} charges, possibly stabilizing configurations such as $Mn^{5+}-N-Li-N-Mn^{5+}$ and promoting local segregation between LiO_4 and Li−Mn−N regions.

As the manganese content in the structure increases, the first effect we observe is that the spectra become noticeably more complex, with broader and more asymmetric peaks (Figure 5), a consequence of the existence of a greater variety of environments. Interestingly, the highest peak is still that around 330 ppm, indicating that the environments with one manganese ion at 109° are still the most frequent. In contrast, the resonance at −260 ppm, related to one manganese ion at 180°, becomes quite broad and noticeably decreases in intensity, likely a consequence of these environments becoming less frequent. Finally, there is an increase of intensity in the resonances because of the existence of environments with several Li−N−Mn interactions, above 800 ppm (e.g., 3 Mn^{5+} at 109°, for 990 ppm, or 2 Mn^{5+} at 70°, for 950 ppm). Nevertheless, no environments above 1000 ppm are observed even at high manganese concentrations, consistent with either a total lack of environments with four manganese ions, or the existence of, at least, one out of the four Mn at 180°, which contributes a negative shift to the overall peak position. This is in contrast to Li_7MnN_4, where an environment with four manganese forming interactions close to 109° does exist. Thus, it appears that, despite the existence of local ordering, this ordering is not identical to that found in Li_7MnN_4, consistent with the observation that the nitride is not part of this solid solution oxynitride series.

Electrochemical Properties. The performance as electrodes in lithium batteries of the oxynitride phases prepared in this study was tested at C/10 rate (where "C" is defined as 1 Li^+ ion extracted/inserted per formula unit in 1 h). The first charge−discharge cycle and a second charge between 3 and 0 V of batteries containing $Li_{12.6}MnN_{3.5}O_{3.6}$, $Li_{17.1}MnN_{3.6}O_{5.7}$, $Li_{28.7}MnN_{3.6}O_{11.5}$, and $Li_{55.6}MnN_{4.4}O_{23.7}$ (samples 5, 9, 11, and 15, respectively), and between 4 and 0 V for $Li_{7.9}MnN_{3.2}O_{1.6}$ are shown in Figure 8 as an example. A broad voltage window was selected to address whether the potentials at which the reactions may take place are affected by the introduction of oxygen in the structure.

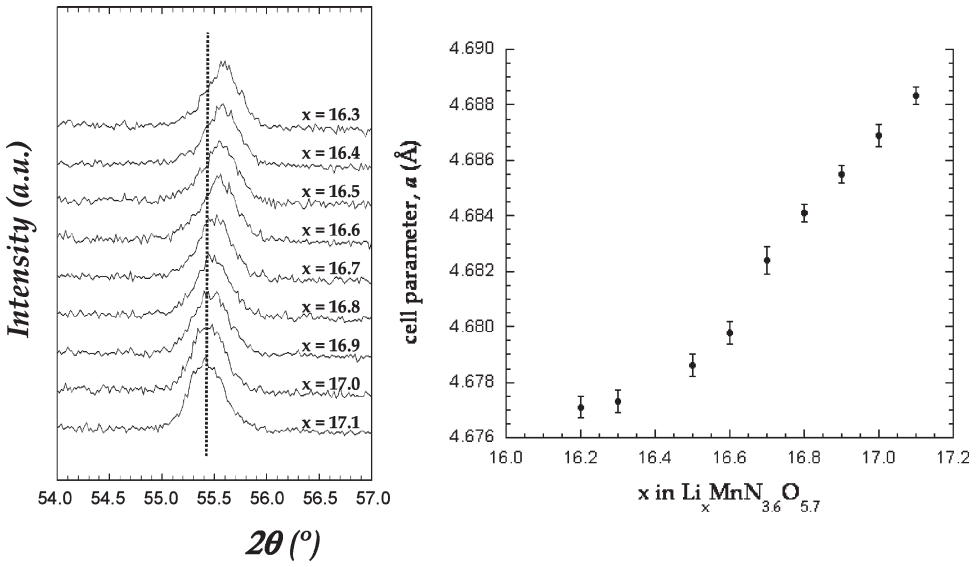

Figure 9. Left: Evolution of the 55°, 2θ reflection in the XRD pattern of $Li_{17.1}MnN_{3.5}O_{3.8}$ (sample 10) as lithium is galvanostatically extracted from its structure at a C/10 rate. The lithium content corresponding to each pattern is indicated. Right: Plot of the evolution of the cell parameter, as calculated from the corresponding XRD patterns, against the lithium content in the sample.

Below 2 V, lithium extraction takes place, for most of the samples, concomitant to a slow but steady increase in voltage up to about 1.4 V, where a slope change occurs and the voltage sharply goes up. As already shown for $Li_{7.9}MnN_{3.2}O_{1.6}$,[17] the mechanism of this lithium extraction is single phase. A total of around 1.2−1.4 lithium ions per formula unit can be deintercalated from $Li_{7.9}MnN_{3.2}O_{1.6}$, $Li_{12.6}MnN_{3.5}O_{3.6}$, and $Li_{17.1}MnN_{3.6}O_{5.7}$, indicating that manganese has similar redox activity in all of them. In contrast, only 0.7 lithium ions can be extracted per formula unit in $Li_{28.7}MnN_{3.6}O_{11.5}$. A negligible charge capacity is generated up to 3 V for $Li_{55.6}MnN_{4.4}O_{23.7}$, which implies that lithium cannot be extracted from its structure at these voltages. Tests with larger voltage windows were attempted but still no lithium extraction was observed for this sample. Thus, there seems to be a decrease in the electroactivity of manganese in these compounds as more lithium and oxygen are put in the structure; that is, as the redox centers, the [MnN_4] units, are more electronically isolated as we move toward the inactivity of the final member of this system, Li_2O.

Other noticeable differences in the processes that take place upon oxidation of the compounds are clearly observable after 2 V. $Li_{7.9}MnN_{3.2}O_{1.6}$, which has the highest nitrogen/manganese content, shows a very long plateau at 2.15 V that leads to very high capacities that cannot be explained solely by the oxidation of the Mn^{5+} ions of the compound to Mn^{7+}. This process results in a complete amorphization of the sample, as previously evaluated by in situ XRD (see the Supporting Information, Figure S1),[52] and was also observed for Li_7MnN_4, although at a lower voltage (ca. 1.8 V).[46] As the lithium and oxygen contents increase, this plateau shortens and increases in voltage slightly (around 2.3 V for $Li_{12.6}MnN_{3.5}O_{3.6}$) until it completely disappears for $Li_{17.1}MnN_{3.6}O_{5.7}$, indicating that it is associated to the presence of large amounts of manganese and nitrogen in the compound. As expected, in situ XRD experiments prove that no amorphization takes place, and only a smooth decrease of the cell parameter, consistent with lithium extraction, was seen

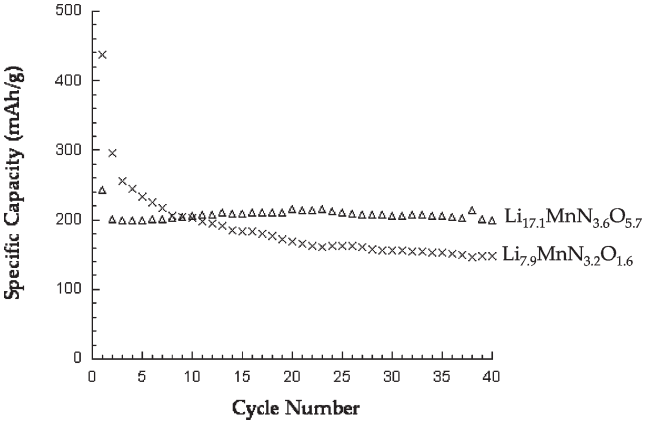

Figure 10. Specific charge capacity vs cycle number resulting from the galvanostatic cycling against lithium metal, at a C/10 rate, of $Li_{7.9}MnN_{3.2}O_{1.6}$ and $Li_{17.1}MnN_{3.6}O_{5.7}$, (samples 1 and 9). $Li_{7.9}MnN_{3.2}O_{1.6}$ was cycled between 4 and 0 V, whereas $Li_{17.1}MnN_{3.6}O_{5.7}$ was cycled between 3 and 0 V.

(Figure 9). Similar amorphization processes were also reported for $Li_{3-x}M_xN$ (M = Fe, Ni, Co, Cu; $0.5 \leq x \leq 0.3$)[66,67] at lower voltages (1.1−1.2 V). Electron Energy Loss Spectroscopy measurements for $Li_{2.6}Co_{0.4}N$ have shown that holes are induced in the N 2p orbitals as lithium is electrochemically deintercalated in this region, which provides evidence for the key role of the pnictide ions in the electrochemical activity of these phases.[68]

The voltage profiles of the first discharge and the second charge are an indication of the major reorganization induced by the processes taking place at 2 V, since the plateau is no longer reproduced in these (and subsequent) current sweeps. The discharge curves for $Li_{17.1}MnN_{3.6}O_{5.7}$ and $Li_{28.7}MnN_{3.6}O_{11.5}$ are virtually symmetric

(66) Nishijima, M.; Kagokashi, T.; Takeda, Y.; Imanishi, M.; Yamamoto, O. *J. Power Sources* **1997**, *68*, 510–514.
(67) Rowsell, J. L. C.; Pralong, V.; Nazar, L. F. *J. Am. Chem. Soc.* **2001**, *123*, 8598–8599.
(68) Suzuki, S.; Shodai, T.; Yamaki, J. *J. Phys. Chem. Solids* **1998**, *59*, 331–336.

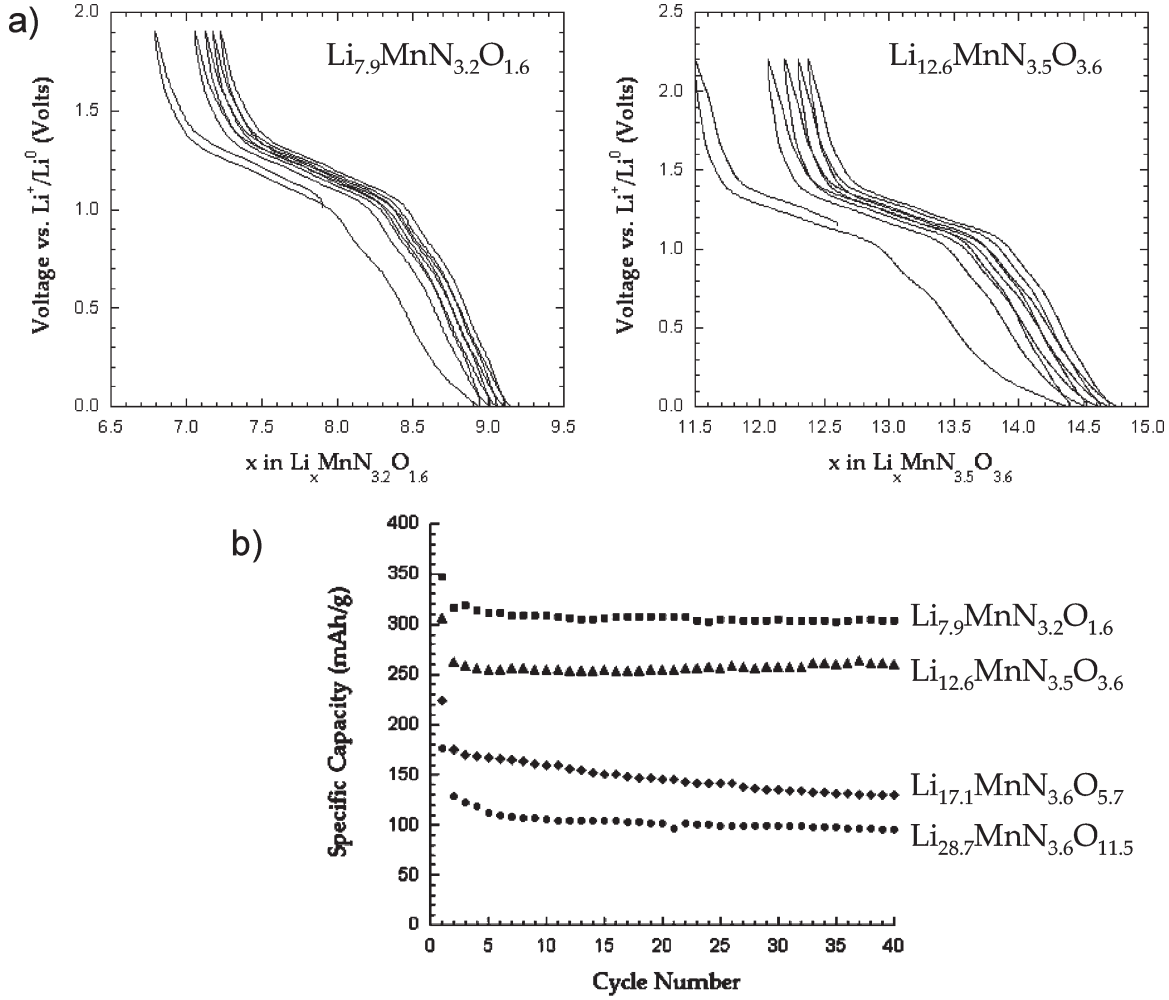

Figure 11. (a) Voltage vs composition profiles of the first 5 cycles of lithium batteries containing $Li_{7.9}MnN_{3.2}O_{1.6}$ and $Li_{12.6}MnN_{3.5}O_{3.6}$ (samples 1 and 5, respectively, as labeled) as electrodes, tested in galvanostatic mode at C/10 rate. $Li_{7.9}MnN_{3.2}O_{1.6}$ was cycled between 1.9 and 0 V, whereas $Li_{12.6}MnN_{3.5}O_{3.6}$ was cycled between 2.2 and 0 V. (b) Specific charge capacity vs cycle number resulting from the cycling of selected samples (as labeled) prepared in this study. $Li_{7.9}MnN_{3.2}O_{1.6}$ (sample 1) was cycled between 1.9 and 0 V, $Li_{17.1}MnN_{3.6}O_{5.7}$ (sample 9) was cycled between 2 and 0 V, and $Li_{12.6}MnN_{3.5}O_{3.6}$ (sample 5) and $Li_{28.7}MnN_{3.6}O_{11.5}$ (sample 11) were cycled between 2.2 and 0 V.

to those of the first charge, a proof of the good reversibility of the single phase electrochemical lithium extraction.

Figure 10 depicts the comparison of the cycling performance between 3 and 0 V at C/10 of $Li_{7.9}MnN_{3.2}O_{1.6}$, which shows the 2 V plateau in the first charge, and $Li_{17.1}MnN_{3.6}O_{5.7}$, which does not. Although higher initial capacity (approximately 440 mAh/g) is found for the former, the structural and microstructural changes that result from the amorphization at those voltages are detrimental for the cyclability, and only 150 mAh/g (35% retention) are obtained after 40 cycles. In contrast, even though the initial capacity of $Li_{17.1}MnN_{3.6}O_{5.7}$ is only 243 mAh/g, the absence of amorphization leads to a much better retention: 83%, with a capacity 200 mAh/g after 40 cycles. Further, most of the 17% capacity loss takes place between cycles 1 and 2, where a voltage response, most likely related to the irreversible Solid Electrolyte Interphase (SEI) formation on the SP carbon that is added to the electrode mixture as a conducting additive, is observed at 0.8 V. Hence, the single-phase electrochemical reaction of the oxynitride is highly reversible.

Given the negative effect of the electrochemical amorphization on the performance of the oxynitride samples prepared in this study, additional cycling experiments using a more limited voltage window were carried out setting the upper cutoff value just below the onset of this process. The first 5 charge−discharge cycles are shown for $Li_{7.9}MnN_{3.2}O_{1.6}$ and $Li_{12.6}MnN_{3.5}O_{3.6}$ in Figure 11a. The curves are comparable to those obtained for $Li_{17.1}MnN_{3.6}O_{5.7}$, for which a restricted cutoff was not needed; the profile recorded for the first charge is reproduced symmetrically for the subsequent current sweeps. The reversibility of the processes that take place at these voltages has a corresponding beneficial effect on the cyclability of these phases (Figure 11b); although the initial capacity is slightly lower than when a wider voltage window is used, the retention is greatly improved (from 35% to 86% capacity retained after 40 cycles for $Li_{7.9}MnN_{3.2}O_{1.6}$). Indeed, the specific capacities obtained after 40 cycles for $Li_{7.9}MnN_{3.2}O_{1.6}$ and $Li_{12.6}MnN_{3.5}O_{3.6}$ (303 mAh/g and 260 mAh/g, respectively) are both even higher than that shown for $Li_{17.1}MnN_{3.6}O_{5.7}$ cycling at higher voltages. For comparison purposes, the results of cycling experiments performed on $Li_{17.1}MnN_{3.6}O_{5.7}$ and $Li_{28.7}MnN_{3.6}O_{11.5}$ with an upper cutoff voltage of 2.2 V are also shown in Figure 11b. As expected from the fact

that the formula weight of the samples increases with no increase in the amount of lithium extracted-inserted, the specific capacity decreases as we move toward Li_2O in the series. Nonetheless, the cyclability is in general quite good for all the samples tested, proving these lithium manganese oxynitrides of interest for application as negative electrodes in lithium-ion batteries. Among them, $Li_{7.9}MnN_{3.2}O_{1.6}$ shows the best properties, combining the highest capacity with a steady delivery over several cycles. The structural changes associated with the promising behavior of this compound were discussed previously,[17,41] and its overall properties were found to be superior to those of Li_7MnN_4, both in terms of chemical stability and electrochemical performance. Given that the chemical stability of these phases does not seem to be improved by the introduction of additional oxygen in the structure, $Li_{7.9}MnN_{3.2}O_{1.6}$ still remains as the most attractive candidate for this application.

Conclusions

A series of compounds in the Li−Mn−N−O system were prepared by using Li_3N, Mn_xN, and increasing proportions of Li_2O, which result in samples with higher lithium and oxygen contents. The samples have XRD patterns that are consistent with a disordered antifluorite structure, as opposed to the superstructure observed for Li_7MnN_4. The plotting of the different stoichiometries in a $Li_3N-Li_2O-MnN_x$ ($x\sim1.7$) ternary phase diagram and the changes in cell parameters as a function of the oxygen molar fraction reveals that Li_7MnN_4 is not an end member in the tie-line formed by all the samples and Li_2O. On the basis of these results, a hypothetical "$Li_{4.5}MnN_{3.2}$" nitride is proposed as the other end member. Attempts to synthesize this new nitride were unsuccessful.

The absence of shift of the main edge position in the XANES Mn *K*-edge spectra of the different compounds indicates that all the oxynitrides contain Mn^{5+} ions preferentially coordinated by N^{3-}, forming [MnN_4] tetrahedra, even at high oxygen contents. This is consistent with the ^6Li MAS NMR data, which cannot be explained by a model in which the O/N anions are distributed in a totally random fashion. Instead the spectra can be rationalized based on a model assuming only [MnN_4] groups, although a very weak resonance that was assigned to Li nearby a [MnN_3O] group was seen. Further analysis indicates that a limited degree of short-range order is present, resulting in a minimization of the [Mn_2N_8] clusters that contain Mn−N−Mn bond angles of 70° to avoid Coulombic repulsions of the Mn^{5+} ions. The absence of resonances above 1000 ppm even at higher manganese contents implies that this short-range order is different to that seen in the Li_7MnN_4 supercell, adding further evidence to the fact that the nitride does not belong to the same series as the oxynitrides.

The electrochemical activity of the different compounds as electrode materials in lithium batteries was also evaluated. The amount of lithium that can be extracted and reinserted in the structure of the compounds decreases with the oxygen content, the samples with the highest contents being virtually inactive. Among the samples tested, $Li_{7.9}MnN_{3.2}O_{1.6}$ was shown to be the most promising candidate because of the higher capacity values and improved retention upon cycling with respect to the other members of the series. This oxynitride was also shown to have the highest chemical stability upon exposure to air.

Acknowledgment. The authors are grateful to Prof. J.-M. Tarascon (LRCS, France), for granting access to the in situ XRD equipment; to Dr. M. M. Doeff (LBNL, U.S.A.), for supplying the Li_3MnO_4 used in this study; and to D. Zeng (SUNY Stony Brook, U.S.A.), Dr. M. Ménétrier and Dr. D. Carlier-Larregaray (ICMCB, Bordeaux) for helpful discussions. This work was supported by Ministerio de Ciencia y Tecnología (MAT2005-03925 and MAT2008-04587), the ALISTORE NoE and the NSF via DMR0506120.

Supporting Information Available: In situ XRD results upon lithium extraction from $Li_{7.9}MnN_{3.2}O_{1.6}$. This material is available free of charge via the Internet at http://pubs.acs.org.